Crystal and Band Structures, Bonding, and Optical Properties of Solid Compounds of Alkaline Indium (III) Pyrophosphates $MInP_2O_7$ (M = Na, K, Rb, Cs)

Yongchun Zhang, Wendan Cheng,* Dongsheng Wu, Hao Zhang, Dagui Chen, Yajing Gong, and Zigui Kan

Fujian Institute of Research on the Structure of Matter, Chinese Academy of Sciences, State Key Laboratory of Structural Chemistry, The Graduate School of the Chinese Academy of Sciences, Fuzhou Fujian 350002, PRC

Received May 31, 2004. Revised Manuscript Received July 29, 2004

Ternary indium (III) pyrophosphates with three-dimensional frameworks of $MInP_2O_7$ (M = Na, K, Rb, Cs) have been found, and the crystal structures have been first reported in this paper. The optical and bonding properties were investigated in terms of the absorption and emission spectra, as well as the calculated band structures and density of states. The crystal band structures calculated by the DFT method show that the solid compounds of $MInP_2O_7$ are insulators with direct band gaps, and the calculated average third-order susceptibilities are increasing in the order of K < Rb < Cs in the $MInP_2O_7$ crystal (M = K, Rb, Cs).

1. Introduction

The past years witnessed an increasing interest in the synthesis and characterization of metal phosphates with open framework structure due to their rich structural chemistry and potential applications in catalysis, adsorbents, and ion-exchangers.[1−3] Specially, the interest in the ternary ortho- and pyrophosphates containing alkaline metals along with various other metals has increased considerably. This is due to the possibility of using these compounds in single or polycrystalline form as nonlinear optical materials,[4] solid electrolytes,[5−7] ionic conductors,[8−13] battery electrodes,[14,15] sensors for detection of NO_x in atmospheric environment,[16] etc. In contrast to the well-known aluminophosphates and gallophosphates,[17] ternary alkali metal phosphates containing indium atom are still to be explored besides reported compounds.[18−31] Of them, the $Na_7(InP_2O_7)_4PO_4$ is particularly important due to the high conductivity anisotropy along two principal unequal crystallographic directions.[26] Belkouch and co-workers have given the lattice parameters of $MInP_2O_7$ (M = Na, K, Rb, and Cs),[32] but until now, no X-ray crystal structural determinations support these parameters. The above compounds have been mostly discovered by mild hydrothermal or high-temperature flux-growth method. Addition-

* To whom correspondence should be addressed. E-mail: cwd@ms.fjirsm.ac.cn.

(1) Cao, G.; Hong, H.-G.; Mallouk, T.E. *Acc. Chem. Res.* **1992**, *25* (9), 420−427.
(2) Centi,G.; Trifiro, F.; Ebner, J. R.; Franchetti, V. M. *Chem. Rev.* **1988**, *88* (1), 55−80.
(3) Clearfield, A. *Chem. Rev.* **1988**, *88* (1), 125−148.
(4) Hagerman, M.E.; Poeppelmeier, K. R. *Chem. Mater.* **1995**, *7*, 602−621.
(5) Aono, H.; Sugimoto, E.; Sadaoka, Y.; Imanaka, N.; Adachi, G. *J. Electrochem. Soc.* **1993**, *140*, 1827−1833.
(6) Aono, H.; Sugimoto, E.; Sadaoka, Y.; Imanaka, N.; Adachi, G. *Solid State Ionics* **1993**, *62*, 309−316.
(7) Ivanov-Schitz, A.K.; Nistuk, A. V.; Chaban, N. G. *Solid State Ionics* **2001**, *139*, 153−157.
(8) Boilot, J.P.; Collin, G.; Colomban, P. *J. Solid State Chem.* **1988**, *73*, 160−171.
(9) Aono, H.; Sugimoto, E.; Sadaoka, Y.; Imanaka, N.; Adachi, G. *Chem. Lett.* **1993**, *12*, 2033−2036.
(10) Sanz, F.; Parada, C.; Rojo, J.M.; Ruiz-Valero, C.; Saez-Puche, R. *J. Solid State Chem.* **1999**, *145*, 604−611.
(11) Dridi, N.; Boukhari, A.; Re'au, J.M.; Arbib, E.; Holt, E. M. *Solid State Ionics* **2000**, *127*, 141−149.
(12) Laghzizil, A.; Barboux, P.; Bouhaouss, A. *Solid State Ionics* **2000**, *128*, 177−181.
(13) Catti, M.; Stramare, S. *Solid State Ionics* **2000**, *136−137*, 489−494.
(14) Delmas, C.; Nadiri, A.; Soubeyroux, J. L. *Solid State Ionics* **1988**, *28−30*, 419−423.
(15) Yamada, A.; Chung, S.C.; Hinokuma, K. *J. Electrochem. Soc.* **2001**, *148*, A224−A229.
(16) Ono, M.; Shimanoe, K.; Miura, N.; Yamazoe, N. *Solid State Ionics* **2000**, *136−137*, 583−588.
(17) Cheetham, A.K.; FeHrey, G.; Loiseau, T. *Angew. Chem., Int. Ed.* **1999**, *38*, 3269−3292.
(18) Tran Qui, D.; Hamdoune, S.; le Page, Y. *Acta Crystallogr. Sect. C* **1987**, *43*, 201−202.
(19) Tran Qui, D.; Hamdoune, S. *Acta Crystallogr. Sect. C* **1987**, *43*, 397−399.
(20) Genkina, E. A.; Muradyan, L. A.; Maksimov, B. A.; Merinov, B. V.; Sigarev, S. E. *Kristallografiya* **1987**, *32*, 74−78.
(21) Lii, K.-H, *Eur. J. Solid State Inorg. Chem.* **1996**, *33*, 519−526.
(22) Zhizhin, M.G.; Komissarova, L. N.; Lazoryak, B. I.; Spiridonov, F. M. *Dokl. Akad. Nauk* **1999**, *365*, 61−63.
(23) Zhizhin, M. G.; Morozov, V. A.; Bobylev, A. P.; Popov, A. M.; Spiridonov, F. M.; Komissarov, L. N.; Lazoryak, B. I. *J. Solid State Chem.* **2000**, *149*, 99−106.
(24) Lii, K.-H.; Ye, J. *J. Solid State Chem* **1997**, *131*, 131−137.
(25) Nagornyi, P. G. *Dopov. Nats. Akad. Nauk. Ukr.* **1998**, *1998*, 141−146.
(26) Stus', N.V.; Lisnyak, V. V.; Nagornyi, P. G. *J. Alloys Compd.* **2001**, *314*, 62−66.
(27) Attfield, M.P.; Cheetham, A. K.; Natarajan, S. *Mater. Res. Bull.* **2000**, *35*, 1007−1015.
(28) Mi, J.-X.; Huang, Y.-X.; Mao, S.-Y.; Huang, X.-D.; Wei, Z.-B.; Huang, Z.-L.; Zhao, J.-T *J. Solid State Chem.* **2001**, *157*, 213−219.
(29) Lii, K.-H. *J. Chem. Soc., Dalton Trans.* **1996**, (6), 815−818.
(30) Dhingra, S.S.; Haushalter, R. C. *J. Solid State Chem.* **1994**, *112*, 96−99.
(31) Murashova, E.V.; Chudinova, N. N. *Inorg. Mater.* **2001**, *37* (12), 1298−1301.
(32) Belkouch, J.; Monceaux, L.; Bordes, E.; Courtine, P. *Mater. Res. Bull.* **1995**, *30* (2), 149−160.

10.1021/cm0491330 CCC: $27.50
Published on Web 09/22/2004

Table 1. Crystal Data and Structure Refinement Parameters for $MInP_2O_7$ (M = Na, K, Rb, Cs)

compound	$NaInP_2O_7$	$KInP_2O_7$	$RbInP_2O_7$	$CsInP_2O_7$
formula weight	311.75	327.86	374.23	421.67
crystal system	monoclinic	monoclinic	monoclinic	monoclinic
space group	P2(1)/c	P2(1)/c	P2(1)/c	P2(1)/c
a (Å)	7.5003(17)	7.4173(15)	7.55230(10)	7.741(14)
b (Å)	8.1774(18)	10.407(2)	10.4201(3)	10.360(9)
c (Å)	9.835(2)	8.4050(17)	8.5026(2)	8.597(9)
β (deg)	112.136(3)	106.223(3)	105.4330(10)	104.57(4)
V (Å^3)	558.8(2)	622.9(2)	644.99(3)	667.3(15)
Z	4	4	4	4
D_c (g/cm^3)	3.706	3.496	3.854	4.197
absorption correction	empirical	empirical	empirical	multiscan
absorption coefficient (mm^{-1})	4.863	4.962	11.645	9.385
crystal dimensions (mm)	0.26 × 0.18 × 0.16	0.19 × 0.14 × 0.12	0.44 × 0.25 × 0.18	0.40 × 0.31 × 0.22
F(000)	584.0	616.0	688.0	760.0
θ ranges for data collected (deg)	2.93−25.05	2.86−25.06	2.80−31.50	2.72−27.48
limiting indices	(−8, −5, −11) to (8, 9, 8)	(−8, −10, −9) to (2, 12, 9)	(−11, −15, −12) to (6, 15, 12)	(−9, −13, −11) to (10, 13, 9)
R_{int}	0.0200	0.0352	0.0466	0.0226
reflections collected	1624	1778	6246	5516
independent reflections	976	1084	2141	1493
parameter/restraints/data (obs.)	101/0/824	96/0/966	101/0/2024	101/0/1453
GOF on F^2	1.067	1.176	1.146	1.106
final R indices	R1 = 0.0354	R1 = 0.0524	R1 = 0.0376	R1 = 0.0200
	R2 = 0.0954	R2 = 0.1368	R2 = 0.0967	R2 = 0.0516
R indices (all data)	R1 = 0.0434	R1 = 0.0609	R1 = 0.0404	R1 = 0.0211
	R2 = 0.1034	R2 = 0.1478	R2 = 0.0984	R2 = 0.0521
largest difference peak and hole (e A^{-3})	1.202 and −1.535	1.843 and −2.172	2.692 and −3.447	1.679 and −1.205

ally, the band structures and optical properties of the typical solid compounds have been seldom reported in contrast to the alkali metal titanyl phosphates, which are mostly investigated in these respects.[33−35]

In this work, we will present synthesis, crystal structure determinations, and spectral measurements for indium pyrophosphates $MInP_2O_7$ (M = Na, K, Rb, and Cs). At the same time, we will make the calculations of crystal energy band structures and optical response functions to understand the chemical bonding properties and electronic origin of optical transition for the solid compounds.

2. Experimental and Computational Procedures

2.1 Crystal Growths. The single-crystals of $MInP_2O_7$ (M = Na, K, Rb, Cs) were prepared by solid-state reactions among analytical grade In_2O_3, $NH_4H_2PO_4$, and either M_2CO_3 (M = Na, Rb, Cs) or MNO_3 (M = K) in a molar ratio corresponding to In/P/M=1:9:11. The samples were ground, heated in air at 923 K for 10 h, and afterward heated at 1273 K (M = Na, K, Rb) or 1223 K (M = Cs) for 24 h in a platinum crucible. The mixtures then were cooled to 1023 K at a rate of 2 K/h and finally quenched to room temperature. Some colorless crystals were selected carefully.

2.2 Crystal Structure Determinations. Single crystals of $MInP_2O_7$ having dimensions 0.26 × 0.18 × 0.16 mm^3 (M = Na), 0.19 × 0.14 × 0.12 mm^3 (M = K), 0.44 × 0.25 × 0.18 mm^3 (M = Rb), and 0.40 × 0.31 × 0.22 mm^3 (M = Cs) were selected for intensity data. The data were collected on a Siemens SMART CCD diffractometer with graphite monochromated Mo Ka radiation (λ = 0.71073 Å) at the temperature of 293 K using the scan mode. Lorentz and polarization corrections were applied to the data. The systematic extinctions, $h0l$: l = 2n; $0k0$: k = 2n; $00l$: l = 2n, are consistent with the space group P2(1)/c. We determined the crystal structures of $MInP_2O_7$ (M = Na, K, Rb, Cs) in terms of the SHELXL[36] software. The positions of metal atoms were located by application of the direct methods with SHELXL program; the remaining atoms were located in succeeding difference Fourier synthesis. Table 1 lists details of cell parameters, data acquisition, and structure solution. The atomic coordinates and thermal parameters are listed in Table 2. Selected bond distances and angles are given in Table 3.

2.3 Spectral Measurements. The samples used for spectral measurements were prepared from pressed abradant of selected micro crystals. To give evidence that it contains pure phase of sample, we determined the powder XRD patterns of $MInP_2O_7$ (M = Na, K, Rb, Cs) using an X'Pert diffractometer with a monochromated Cu Kα X-ray source (step size of 0.02° and range 2θ = 10−80°). Figure 1 gives the powder X-ray diffraction patterns of $MInP_2O_7$ (M = Na, Rb). These patterns compare with those simulated by the program Visualizer Software using the crystallographic data, confirming the monophasic nature of the prepared samples. The absorption spectrum was recorded by a UV-3101PC spectrometer at 300 K from 200 to 2000 nm, and the luminescence was measured by a FL/FS 900 time-resolved fluorescence spectrometer using a Xe lamp at room temperature for $MInP_2O_7$ (M = Na, K, Rb, Cs) solid compounds.

2.4 Computational Descriptions. The crystallographic data of four ternary indium (III) pyrophosphates $MInP_2O_7$ (M = Na, K, Rb, Cs) determined by X-ray were used to calculate electronic band structures of the solid compounds. The calculations of band structures were made by the density functional theory (DFT) with local gradient-corrected exchange-correlation functional[37] and performed with the CASTEP code,[38,39] which uses a plane wave basis set for the valence electrons and norm-conserving pseudopotential[40] for the core states. The number of plane waves included into the basis was determined by a cutoff energy of 450 eV. Pseudo atomic calculations were

(33) Ching, W. Y.; Xu, Y.-N. *Phys. Rev. B*, **1991**, *44* (10), 5332−5335.
(34) Zumsteg, F. C.; Bierlein, J. D.; Gier, T. E., *J. Appl. Phys.* **1976**, *47* (11), 4980−4985.
(35) Phillips, M. L.; Gier, T. E.; Eddy, M. M.; Keder, N. L.; Stucky, G. D.; Bierlein, J. D. *Solid State Ionics* **1989**, *32−33*, 147−153.
(36) Sheldrick G. M. In *Crystallographic Computing 3*; Sheldrick, G. M., Krüger, C., Goddard, R., Eds.; Oxford University Press: New York, 1985; pp 175−189.
(37) Perdew, J. P.; Burke, K.; Ernzerhof, M. *Phys. Rev. Lett.* **1996**, *77*, 3865−3868.
(38) Segall, M.; Lindan, P.; Probert, M.; Pickard, C.; Hasnip, P.; Clark, S.; Payne, M. *Materials Studio CASTEP*, version 2.2, 2002.
(39) Segall, M. D.; Lindan, P. L. D.; Probert, M. J.; Pickard, C. J.; Hasnip, P. J.; Clark, S. J. Payne, M. C. *J. Phys.: Cond. Matt.* **2002**, *14*, 2717−2744.
(40) Hamann, D. R.; Schluter, M.; Chiang, C. *Phys. Rev. Lett.* **1979**, *43*, 1494−1497.

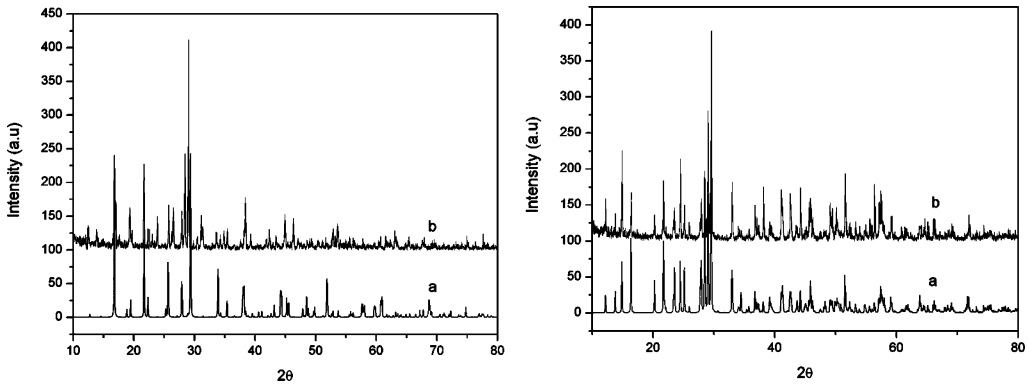

Figure 1. Simulated (a) and experimental (b) powder X-ray (Cu Kα) diffraction patterns for $NaInP_2O_7$ (left) and $RbInP_2O_7$ (right).

Table 2. Fractional Atomic Coordinates and Equivalent Isotropic Displacement Parameters

atom	*X*	*Y*	*Z*	U_{eq}[a]
		$NaInP_2O_7$		
In	0.74432(5)	−0.00465(4)	0.24997(4)	0.0068(3)
Na	1.2825(4)	0.0194(4)	0.2869(4)	0.0259(8)
P1	0.6731(2)	0.21652(18)	−0.04611(16)	0.0088(4)
P2	0.9264(2)	−0.24794(18)	0.54005(16)	0.0082(4)
O1	1.0281(6)	0.0896(5)	0.3720(4)	0.0115(9)
O2	0.8200(6)	−0.2224(5)	0.3766(5)	0.0139(10)
O3	0.6257(6)	0.1095(5)	0.3954(5)	0.0132(10)
O4	0.8266(6)	−0.1291(5)	0.0992(4)	0.0169(10)
O5	0.5401(6)	0.0902(5)	−0.1448(4)	0.0125(10)
O6	0.6964(6)	0.2106(5)	0.1133(5)	0.0124(10)
O7	0.8720(5)	0.1660(5)	−0.0617(4)	0.0130(10)
		$KInP_2O_7$		
In	0.76545(9)	0.90057(7)	0.24344(8)	0.0120(4)
K	1.1788(4)	0.8201(3)	0.0565(3)	0.0291(7)
P1	0.8668(4)	0.5972(3)	0.1766(4)	0.0160(7)
P2	0.5551(4)	0.6407(3)	0.3099(3)	0.0134(7)
O1	0.5384(10)	0.7823(7)	0.2658(10)	0.0189(17)
O2	0.9871(10)	0.4940(7)	0.2828(9)	0.0156(16)
O3	0.9261(11)	0.7297(8)	0.2547(12)	0.030(2)
O4	0.6565(11)	0.5707(7)	0.1850(9)	0.0174(16)
O5	0.6762(15)	0.6082(8)	0.4792(11)	0.031(2)
O6	0.3592(12)	0.5834(7)	0.2687(12)	0.028(2)
O7	0.8633(17)	0.5901(12)	0.0024(12)	0.053(4)
		$RbInP_2O_7$		
In	0.73611(3)	0.09965(3)	0.25691(3)	0.00467(13)
Rb	0.31339(6)	0.18488(5)	0.44847(5)	0.01685(15)
P1	0.63237(14)	0.09641(9)	0.82559(13)	0.0055(2)
P2	−0.06190(13)	0.13603(10)	0.68712(12)	0.0054(2)
O1	0.5069(4)	−0.0038(3)	0.7220(4)	0.0087(5)
O2	−0.1643(4)	0.0659(3)	0.8077(4)	0.0111(6)
O3	−0.0478(4)	0.2778(3)	0.7308(4)	0.0105(6)
O4	0.5776(4)	0.2301(3)	0.7554(4)	0.0112(6)
O5	0.1311(4)	0.0805(3)	0.7310(4)	0.0126(6)
O6	−0.1753(6)	0.1056(4)	0.5170(4)	0.0186(7)
O7	0.6415(6)	0.0877(4)	1.0018(5)	0.0213(8)
		$CsInP_2O_7$		
In	0.26179(3)	0.398547(19)	0.24233(2)	0.00302(11)
Cs	0.69572(3)	0.29998(2)	0.04195(3)	0.01476(11)
P1	0.36589(11)	0.09154(7)	0.16997(10)	0.00366(17)
P2	0.92768(11)	0.62893(8)	0.18264(9)	0.00362(17)
O1	0.4978(3)	−0.0040(2)	0.2693(3)	0.0075(4)
O2	0.8250(3)	0.5558(2)	0.2990(3)	0.0082(4)
O3	0.4134(3)	0.2277(2)	0.2331(3)	0.0095(5)
O4	0.9422(3)	0.7713(2)	0.2284(3)	0.0088(5)
O5	1.1140(3)	0.5727(2)	0.2250(3)	0.0098(5)
O6	0.3459(4)	0.0790(3)	−0.0070(3)	0.0153(5)
O7	0.8197(4)	0.6022(2)	0.0142(3)	0.0162(6)

[a] $U_{eq} = (1/3)\Sigma_i\Sigma_j U_{ij}\ \mathbf{a_i}^*\mathbf{a_j}^*\mathbf{a_i}\mathbf{a_j}$.

performed for O $2s^22p^4$, P $3s^23p^3$, In $5s^25p^1$, Na $2s^22p^63s^1$, K $3s^23p^64s^1$, Rb $4s^24p^65s^1$, and Cs $5s^25p^66s^1$. The calculating parameters and convergent criteria were set by the default values of CASTEP code.[37] The calculations of linear optical properties described in terms of the complex dielectric function $\epsilon = \epsilon_1 + \epsilon_2$ were also made in this work. The imaginary part of the dielectric function $\epsilon(\omega)_2$) was given in the following equation.[41]

$$\epsilon_2(\omega) = 4(\pi e/m\omega)^2\Sigma_{v,c}\int_{BZ} 2d\mathbf{k}/(2\pi)^3|\mathbf{e}\cdot\mathbf{M}_{cv}(\mathbf{k})|^2 \times \delta(E_c(\mathbf{K}) - E_v(\mathbf{K}) - \hbar\omega) \quad (1)$$

The symbol Σ is summation over the valence bands (v) and conduction bands (c), and the symbol $\int$ is integration over **k** vectors in Brillouin zone (BZ). The $\mathbf{e}\cdot\mathbf{M}_{cv}(\mathbf{k})$ is an electron transition moment between the conduction and valence bands at the **k** point, and the argument of the δ function is the energy difference between the conduction and valence bands at **k** point with absorption of a quantum $\hbar\omega$, $(E_c(\mathbf{K}) - E_v(\mathbf{K}) - \hbar\omega)$.

CASTEP calculated the real $\epsilon(\omega)_1$ and imaginary $\epsilon(\omega)_2$) parts of the dielectric function.[38] The $\epsilon(\omega)_2$ can be thought of as detailing the real transitions between occupied and unoccupied electronic states. The real and imaginary parts were linked by a Kramers−Kronig transform.[41] This transform was used to obtain the real part $\epsilon(\omega)_1$ of the dielectric function.

The first-order nonresonant susceptibility at low-frequency region was given by $\chi^{(1)}(\omega)_{ii} = [\epsilon(\omega)_{ii} - 1]/4\pi$, and third-order nonresonant susceptibility can be expressed in terms of the first-order susceptibilities at the four different frequencies ω_q, ω_m, ω_n, and ω_p as follows:

$$\chi^{(3)}{}_{ijkl}(-\omega_q; \omega_m, \omega_n, \omega_p) = (\omega_0/d)^2 m/(3N^3e^4) \times [\chi^{(1)}{}_{ii}(\omega_q)\,\chi^{(1)}{}_{jj}(\omega_m)\,\chi^{(1)}{}_{kk}(\omega_n)\,\chi^{(1)}{}_{ll}(\omega_p)] \times [\delta_{ij}\delta_{kl} + \delta_{ik}\delta_{jl} + \delta_{il}\delta_{jk}] \quad (2)$$

The expression is derived from a classical anharmonic oscillator (CAHO) model[42] in which *m* and *e* are, respectively, electron mass and charge. The lattice constant *d* and frequency ω_0 are, respectively, 3 Å and 1 × 1016 rad/sec, and *N* is unit cell density number with units of cm^{-3} in the present study.

3. Results and Discussions

3.1 Crystal Structures of $NaInP_2O_7$ and $MInP_2O_7$ (M = K, Rb, Cs). The structure of $NaInP_2O_7$ is illustrated in Figure 2. It consists of a three-dimensional framework of corner sharing InO_6 octahedra and P_2O_7 groups. The sodium ions are located in infinite channels running along [1 0 1] with 6-sided windows, each of which is formed by the edges of two InO_6 octahedra and four PO_4 tetrahedra. Lateral 3-sided windows are also observed, but they are not of enough space to permit sodium ions to migrate through. Each InO_6 octahedron

(41) Bassani, F.; Parravicini, G. P. *Electronic States and Optical Transitions In Solids;* Pergamon Press Ltd.: Oxford, 1975; pp149−154.

(42) Boyd, R. W. *Nonlinear Optics* Academic Press: New York, 1992, pp 21−32.

Table 3. Selected Interatomic Distances (Å) and Angles (deg) for $MInP_2O_7$ (M = Na, K, Rb, Cs)

				$NaInP_2O_7$ [a]			
In−O4	2.075(5)	In−O6	2.161(4)	P2−O4v	1.496(5)	Na−O5iv	2.435(7)
In−O5i	2.109(5)	P1−O5	1.508(4)	P2−O2	1.516(5)	Na−O3viii	2.498(6)
In−O2	2.124(4)	P1−O6	1.511(5)	P2−O1vi	1.523(4)	Na−O7iv	2.572(6)
In−O1	2.154(5)	P1−O3iii	1.526(4)	P2−O7vii	1.608(4)	Na−O2ix	2.589(6)
In−O3	2.160(6)	P1−O7	1.610(4)	Na−O1	2.424(7)	Na−O6vii	2.692(5)
O4−In−O5i	90.29(16)	O5i−In−O3	82.83(17)	O3−In−O6	92.66(17)	O4v−P2−O2	111.37(24)
O4−In−O2	85.53(16)	O2−In−O3	93.43(17)	O5−P1−O6	115.82(24)	O4v−P2−O1vi	112.86(24)
O5i−In−O2	90.40(17)	O1−In−O3	92.49(17)	O5−P1−O3iii	113.11(24)	O2−P2−O1vi	113.64(23)
O4−In−O1	94.37(16)	O4−In−O6	88.83(16)	O6−P1−O3iii	109.90(25)	O4v−P2−O7vii	103.75(25)
O5i−In−O1	175.25(17)	O5i−In−O6	93.71(16)	O5−P1−O7	100.07(24)	O2−P2−O7vii	107.09(24)
O2−In−O1	89.06(16)	O2−In−O6	173.04(16)	O6−P1−O7	109.97(24)	O1vi−P2−O7vii	107.38(24)
O4−In−O3	173.04(17)	O1−In−O6	87.30(16)	O3iii−P1−O7	107.22(24)	P2ix−O7−P1	137.23(28)
				$KInP_2O_7$ [b]			
In−O7i	2.095(10)	P1−O7	1.459(11)	K−O1vii	2.782(9)	K−O7	3.289(13)
In−O6ii	2.105(8)	P1−O2	1.517(8)	K−O3	2.986(11)	K−O4iv	3.396(8)
In−O3	2.128(8)	P1−O3	1.538(9)	K−O2iii	3.038(8)	P2−O5	1.494(9)
In−O1	2.136(8)	P1−O4	1.605(9)	K−O6vii	3.115(9)	P2−O1	1.516(8)
In−O5iii	2.135(9)	K−O2iv	2.746(9)	K−O5iv	3.227(9)	P2−O6	1.518(9)
In−O2iv	2.142(8)	K−O3iii	2.749(10)	K−O6viii	3.234(11)	P2−O4	1.625(9)
O7i−In−O6ii	91.63(43)	O6ii−In−O5iii	89.08(35)	O5iii−In−O2iv	86.44(34)	O5−P2−O1	116.05(47)
O7i−In−O3	88.02(43)	O3−In−O5iii	91.01(36)	O7−P1−O2	113.41(54)	O5−P2−O6	114.25(56)
O6ii−In−O3	171.99(31)	O1−In−O5iii	92.52(35)	O7−P1−O3	113.37(59)	O1−P2−O6	108.56(44)
O7i−In−O1	89.32(41)	O7i−In−O2iv	91.59(40)	O2−P1−O3	109.43(46)	O5−P2−O4	104.49(46)
O6ii−In−O1	100.29(30)	O6ii−In−O2iv	87.83(31)	O7−P1−O4	106.88(59)	O1−P2−O4	107.39(43)
O3−In−O1	87.71(30)	O3−In−O2iv	84.18(31)	O2−P1−O4	105.76(44)	O5−P2−O1	116.05(47)
O7i−In−O5iii	177.88(36)	O1−In−O2iv	171.80(29)	O3−P1−O4	107.51(45)	P1−O4−P2	125.62(54)
				$RbInP_2O_7$ [c]			
In−O7i	2.099(4)	Rb−O4	2.871(3)	Rb−O6vi	3.240(4)	P1−O4	1.529(3)
In−O5ii	2.118(3)	Rb−O3v	2.886(3)	Rb−O5	3.257(4)	P1−O2iv	1.615(3)
In−O3iii	2.130(3)	Rb−O1ii	2.924(4)	Rb−O7v	3.371(4)	P2−O6	1.506(3)
In−O6iv	2.134(3)	Rb−O4v	3.034(4)	Rb−O2vi	3.396(3)	P2−O5	1.520(3)
In−O4v	2.138(3)	Rb−O1	3.099(3)	P1−O7	1.484(5)	P2−O3	1.520(3)
In−O1ii	2.138(3)	Rb−O5v	3.152(3)	P1−O1	1.523(3)	P2−O2	1.614(4)
O7i−In−O5ii	91.38(15)	O5ii−In−O4v	173.11(12)	O4v−In−O1ii	84.05(12)	O6−P2−O5	114.77(21)
O7i−In−O3iii	89.28(15)	O3iii−In−O4v	86.86(12)	O7−P1−O1	113.36(21)	O6−P2−O3	115.11(20)
O5ii−In−O3iii	99.81(12)	O6iv−In−O4v	90.16(15)	O7−P1−O4	112.64(21)	O5−P2−O3	108.05(18)
O7i−In−O6iv	177.65(14)	O7i−In−O1ii	89.73(15)	O1−P1−O4	109.69(18)	O6−P2−O2	105.59(19)
O5ii−In−O6iv	87.80(14)	O5ii−In−O1ii	89.30(12)	O7−P1−O2iv	107.05(22)	O5−P2−O2	105.19(17)
O3iii−In−O6iv	93.04(15)	O3iii−In−O1ii	170.85(12)	O1−P1−O2iv	105.75(18)	O3−P2−O2	107.40(17)
O7i−In−O4v	90.40(15)	O6iv−In−O1ii	88.06(15)	O4−P1−O2iv	107.94(17)	P2−O2−P1viii	126.81(21)
				$CsInP_2O_7$ [d]			
Cs−O3i	2.998(75)	Cs−O5iv	3.298(40)	In−O5vii	2.121(4)	P1−O3	1.523(6)
Cs−O4ii	3.010(71)	Cs−O7	3.301(4)	In−O7viii	2.136(25)	P1−O2vi	1.609(10)
Cs−O3	3.138(45)	Cs−O2	3.435(25)	In−O3	2.136(3)	P2−O7	1.504(31)
Cs−O1iii	3.198(30)	Cs−O6	3.490(14)	In−O1iii	2.142(5)	P2−O5	1.513(14)
Cs−O5ii	3.200(36)	In−O6v	2.101(26)	P1−O6	1.496(7)	P2−O4	1.523(3)
Cs−O1i	3.241(43)	In−O4vi	2.120(8)	P1−O1	1.521(22)	P2−O2	1.614(19)
O6v−In−O4vi	89.71(11)	O4vi−In−O3	85.51(10)	O3−In−O1iii	84.08(10)	O7−P2−O5	115.22(16)
O6v−In−O5vii	90.02(11)	O5vii−In−O3	173.55(10)	O6−P1−O1	113.43(15)	O7−P2−O4	114.45(14)
O4vi−In−O5vii	97.62(9)	O7viii−In−O3	88.91(9)	O6−P1−O3	113.38(15)	O5−P2−O4	107.86(14)
O6v−In−O7viii	173.78(10)	O6v−In−O1iii	86.96(11)	O1−P1−O3	109.57(13)	O7−P2−O2	105.61(14)
O4vi−In−O7viii	94.87(10)	O4vi−In−O1iii	168.71(11)	O6−P1−O2vi	106.51(16)	O5−P2−O2	104.97(16)
O5vii−In−O7viii	85.22(9)	O5vii−In−O1iii	93.18(10)	O1−P1−O2vi	105.78(15)	O4−P2−O2	108.07(13)
O6v−In−O3	95.65(11)	O7viii−In−O1iii	89.31(10)	O3−P1−O2vi	107.67(14)	P1iii−O2−P2	127.62(18)

[a] Symmetry codes: (i) $1-x, -y, -z$; (ii) $-1+x, y, z$; (iii) $x, 0.5-y, -0.5+z$; (iv) $2-x, -y, -z$; (v) $x, -0.5-y, 0.5+z$; (vi) $2-x, -y, 1-z$; (vii) $2-x, -0.5+y, 0.5-z$; (viii) $1+x, y, z$; (ix) $2-x, 0.5+y, 0.5-z$; (x) $x, 0.5-y, 0.5+z$; (xi) $x, -0.5-y, -0.5+z$. [b] Symmetry codes: (i) $x, 1.5-y, 0.5+z$; (ii) $1-x, 0.5+y, 0.5-z$; (iii) $x, 1.5-y, -0.5+z$; (iv) $2-x, 0.5+y, 0.5-z$; (v) $2-x, 2-y, -z$; (vi) $2-x, -0.5+y, 0.5-z$; (vii) $1+x, y, z$; (viii) $1+x, 1.5-y, -0.5+z$; (ix) $-1+x, y, z$; (x) $1-x, -0.5+y, 0.5-z$; (xi) $-1+x, 1.5-y, 0.5+z$. [c] Symmetry codes: (i) $x, y, -1+z$; (ii) $1-x, -y, 1-z$; (iii) $1+x, 0.5-y, -0.5+z$; (iv) $1+x, y, z$; (v) $x, 0.5-y, -0.5+z$; (vi) $-x, -y, 1-z$; (vii) $x, 0.5-y, 0.5+z$; (viii) $-1+x, y, z$; (ix) $-1+x, 0.5-y, 0.5+z$; (x) $x, y, 1+z$. [d] Symmetry codes: (i) $x, 0.5-y, -0.5+z$; (ii) $2-x, -0.5+y, 0.5-z$; (iii) $1-x, 0.5+y, 0.5-z$; (iv) $2-x, 1-y, -z$; (v) $x, 0.5-y, 0.5+z$; (vi) $1-x, -0.5+y, 0.5-z$; (vii) $-1+x, y, z$; (viii) $1-x, 1-y, -z$; (ix) $2-x, 0.5+y, 0.5-z$; (x) $1+x, y, z$.

is linked to five different P_2O_7 groups, and each P_2O_7 group shares its six corners with five different InO_6 octahedra and is bonded to one of the InO_6 octahedra through bidentate bonding. The InO_6 octahedra are little distorted as indicated from the In−O distances {2.075(5)−2.161(4) Å} and O−In−O bond angles {82.83(17)−94.37(16)°}. The expected In−O distance from the effective ionic radii reported by Shannon is 2.15 Å.[43] The two PO_4 tetrahedra of a P_2O_7 group are in a semieclipsed configuration (Figure 3a) as in the isostructural diphosphate involving lithium,[18] and they present the features usually observed in other diphos-

(43) Shannon, R. D. *Acta Crystallogr.* **1976**, *A32*, 751−767.

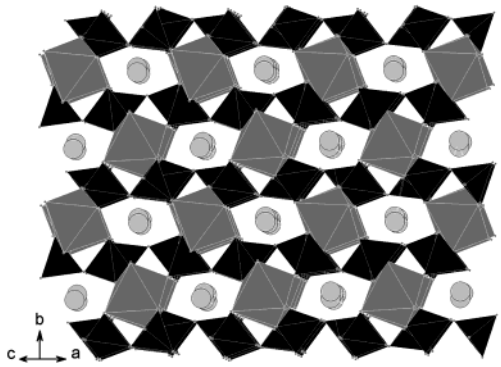

Figure 2. Projection along [1 0 1] illustrating the 6-MR channels containing the sodium atoms: indium ocathedra are medium gray; phosphorus tetrahedra are black; sodium cations are indicated by the light gray circles.

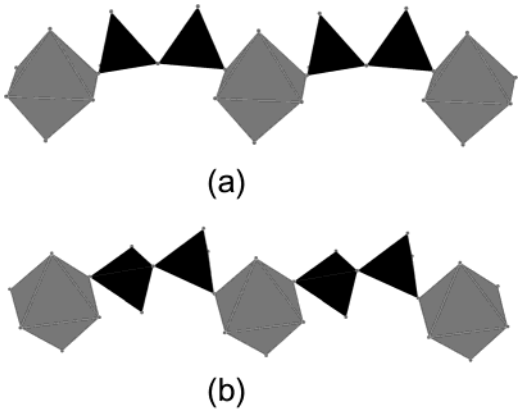

Figure 3. Strings of corner sharing octahedral and diphosphate groups in (a) $NaInP_2O_7$ and (b) $RbInP_2O_7$: the PO_4 tetrahedra are black and InO_6 octahedra are medium gray.

phates: the $P-O_{terminal}$ distances {average 1.513(8) Å} are shorter than $P-O_{bridging}$ bonds {average 1.609(4) Å compared to Shannon's 1.52 Å[43]}. The O−P−O angles show distortion from idealized tetrahedral geometry {103.75(25)−115.82(24)°} and the P−O−P bond angles involving the bridging oxygen {137.23(28)°} are greater than that in the Li compound {132.75(37)°}. This mixed framework delimits cages elongated along [1 0 1] where the Na^+ are located. Each Na^+ ion is coordinated by six O atoms at distances ranging from 2.424(7) to 2.692(5) Å compared to Shannon's 2.37 Å.[43]

As shown in Figure 4, the compounds $MInP_2O_7$ (M = K, Rb, Cs) possess three-dimensional $(InP_2O_7)^-$ anionic frameworks with one-dimensional tunnels occupied by cations, K^+, Rb^+, or Cs^+. Since the features of the anionic frameworks that built up from corner sharing InO_6 octahedra and PO_4 tetrahedra are the same, we discuss these structures by taking $RbInP_2O_7$ as an example. In $RbInP_2O_7$, the tunnels running along [0 0 1] result from stacking of rings formed by the edges of three octahedra and four tetrahedra (Figure 5). Adjacent layers are generated by c-glide plane and these layers form a three-dimensional network with tunnels running along the *c*-axis.

The Rb^+ cations are located in these tunnels, realizing a 10-fold coordination with Rb−O distances ranging from 2.871(3) to 3.396(3) Å compared to Shannon's 3.01 Å.[43]

Each InO_6 group is connected, via In−O−P bonds, to five P_2O_7 groups: two corners of the InO_6 octahedron

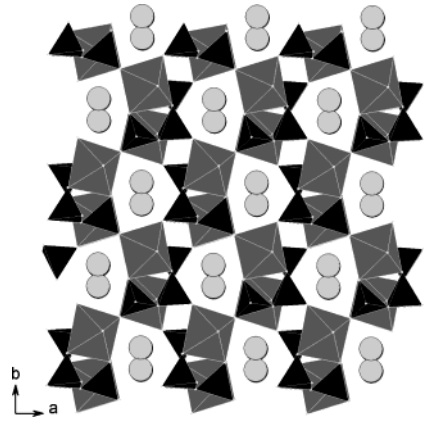

Figure 4. Framework structure of $MInP_2O_7$ (M = K, Rb, Cs) along [0 0 1]: indium ocathedra are medium gray; phosphorus tetrahedra are black; the light gray circles represent potassium, rubidium, or cesium cations.

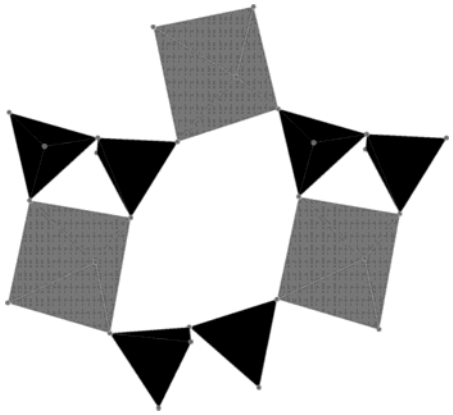

Figure 5. Projection along the [0 0 1] direction of a $[InP_2O_7]^-$ layer in $RbInP_2O_7$: the PO_4 tetrahedra are black and InO_6 octahedra are medium gray.

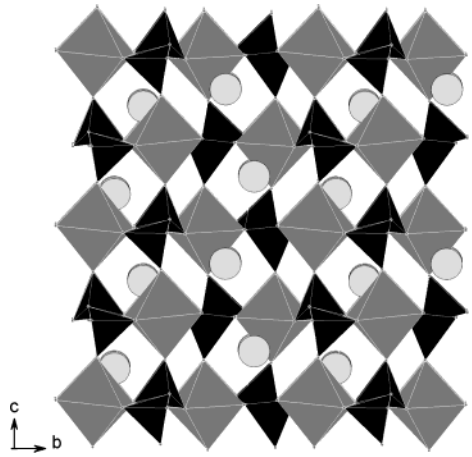

Figure 6. Projection along [1 0 0] showing the connection between $[InP_2O_7]^\infty$ layers in $RbInP_2O_7$: indium ocathedra are medium gray; phosphorus tetrahedra are black; rubidium atoms are indicated by the light gray circles.

are linked to one P_2O_7 group and the other four corners connect with four distinct P_2O_7 groups. The InO_6 octahedra are also distorted as shown by the In−O distances ranging from 2.099(4) to 2.138(3) Å compared to Shannon's 2.15 Å[43] and O−In−O bond angles ranging from 84.05(12)° to 99.81(12)°. In contrast to the eclipsed P_2O_7 groups in $NaInP_2O_7$, the diphosphate groups in $RbInP_2O_7$ present a staggered configuration (Figure 3b),

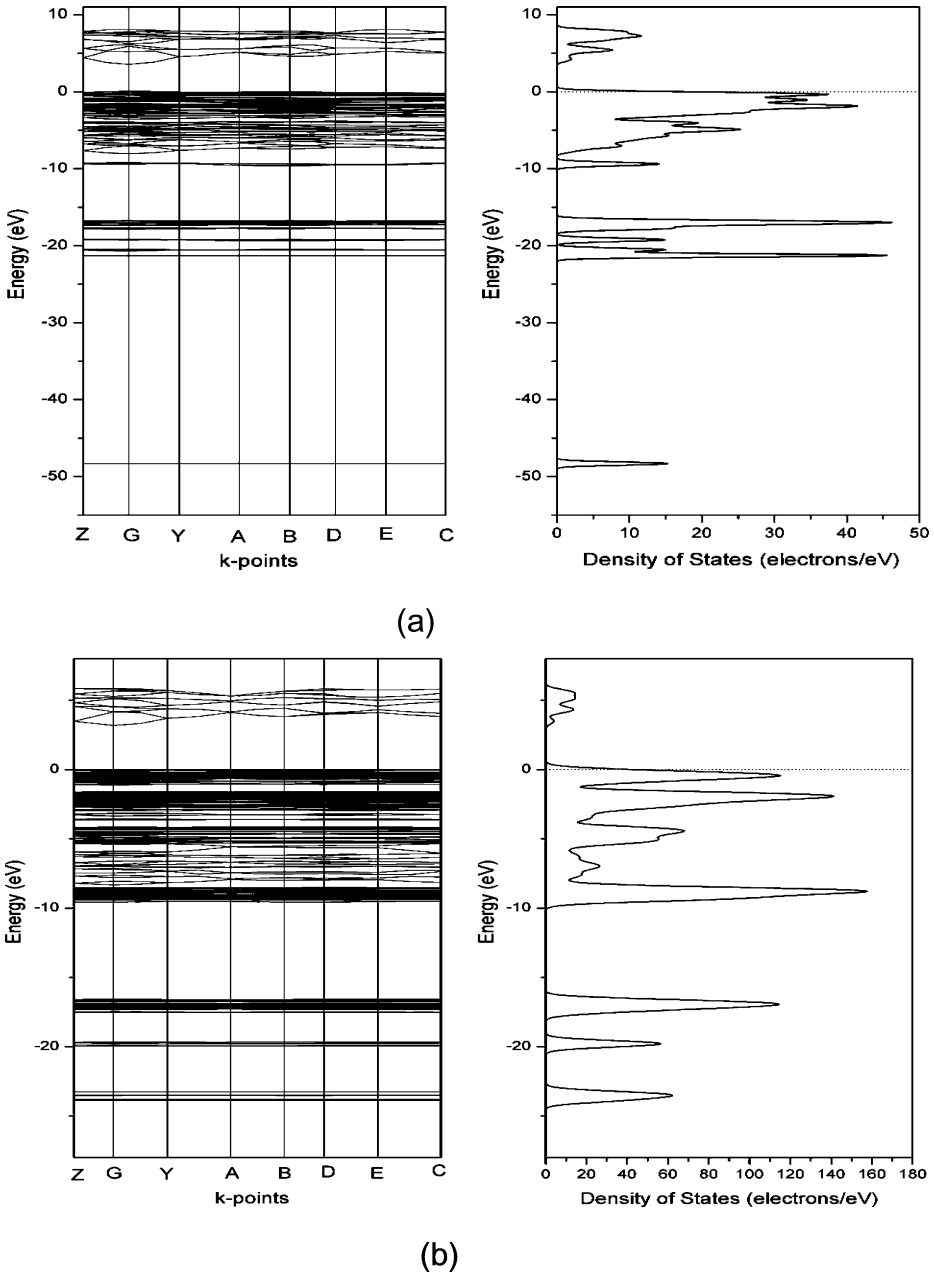

Figure 7. Energy band structures and density of states: (a) $NaInP_2O_7$, (b) $RbInP_2O_7$.

one long P−O bond and three much shorter P−O bonds (Table 3). The P−O−P bond angles in $RbInP_2O_7$ {126.81(21)°} are about the same as that in the $KInP_2O_7$ {125.62(54)°} and $CsInP_2O_7$ {127.62(18)°}, but much smaller than that in the Na compound.

In general, the flexibility of the P_2O_7 group is remarkable: it is very adaptive to the bonding requirements of the other groups by adjusting the P−O−P bond angle and the configurations of two PO_4 tetrahedra. This adaptability is perhaps more striking for $MInP_2O_7$ (M = K, Rb, Cs) in that the height of one P_2O_7 group corresponds to that of an octahedron, and one P_2O_7 group alternates with an octahedron (Figure 6).

3.2 Band Structures, Density of States, and Chemical Bonds. The energy band structures and density of states (DOS) have been calculated by the DFT method for the crystals of $MInP_2O_7$ (M = Na, K, Rb, Cs). Figure 7 only gives the band structures and DOS of the $MInP_2O_7$ (M = Na, Rb).

The band structures and DOS of $KInP_2O_7$ and $CsInP_2O_7$ are similar to those of $RbInP_2O_7$. It is shown that the valence bands are flat, and the conduction bands are oscillating. The lowest k-point of conduction band is localized at G point and the direct band gap is at about 3.5, 3.7, 3.7, and 3.7 eV for the $MInP_2O_7$ (M = Na, K, Rb, and Cs), individually. The valence bands between energy −8.0 eV and the Fermi level (0.0 eV) are crowed and mostly formed by the O 2p and P 3p states, but mixings with small In 5s and In 5p states and the valence bands lying about between −21.0 and −16.0 eV are the main contributions from the hybridizations of P 3s and O 2s states for the $MInP_2O_7$ (M = Na, K, Rb, and Cs), respectively. The other valence bands are separate and they are assigned as M valence orbital states. For example, the valence bands localized at about −23.0 and about −8.5 eV are made from Rb 4p and Rb 5s states, respectively, as shown in Figure 8a. The conduction bands localized about between 4.0

Table 4. Calculated Bond Orders and Atomic Charges (*e*) of $MInP_2O_7$ within a Unit Cell

M	M−O	In−O	P−O	average atomic charge
Na	0.02 to 0.07	0.30 to 0.34	0.44 to 0.76	$P^{2.20+}$ $In^{1.93+}$ $Na^{1.00+}$ $O^{1.05-}$
K	to 0.05	0.28 to 0.35	0.46 to 0.75	$P^{2.23+}$ $In^{1.91+}$ $K^{1.05+}$ $O^{1.06-}$
Rb	to 0.03	0.29 to 0.35	0.46 to 0.75	$P^{2.24+}$ $In^{1.87+}$ $Rb^{1.12+}$ $O^{1.07-}$
Cs	0.0	0.30 to 0.37	0.45 to 0.75	$P^{2.22+}$ $In^{1.81+}$ $Cs^{1.20+}$ $O^{1.06-}$

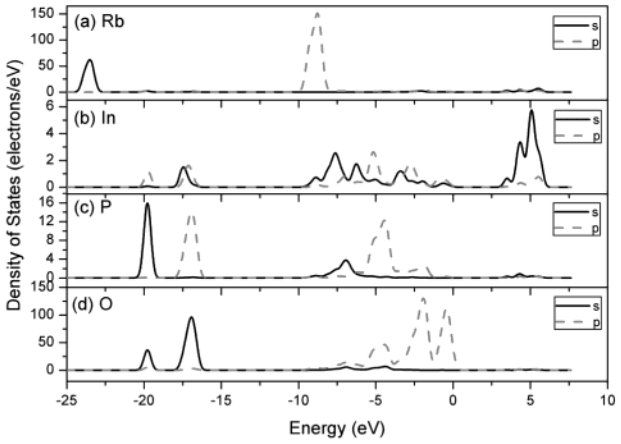

Figure 8. Partial density of states in $RbInP_2O_7$: (a) Rb, (b) In, (c) P, and (d) O atoms.

and 9.0 eV are mainly due to In 5s and In 5p states hybridized with small P 3s and P 3p states.

Furthermore, we have also calculated the atomic site and angular momentum projected DOS of $MInP_2O_7$ (M = Na, K, Rb, Cs) to elucidate the nature of the electronic band structures and chemical bonds. From about −3.2 to 0.0 eV the DOS is higher for O 2p states than P 3p states, and from about −9.0 to −4.0 eV the DOS is lower for In 5p states than O 2p states, while we compare the total DOS in Figure 7 with the angular momentum projected DOS for P 3p and O 2p states displayed in Figure 8. These findings show that some electrons from P 3p and In 5p transform into the valence bands and take part in the strong covalence interactions between P and O atoms, and weak covalence interactions between In and O atoms. It is also found that the DOS is much higher for M *n*s (M = Na, K, Rb, Cs; *n* = 2, 3, 4, 5) state than O 2p state from −8.5 to −7.5 eV, and the electrons from M *n*s states transform into the valence bands and take part in the ionic interactions between M and O atoms mostly. These results are also evidenced from the population analysis. For example, the calculated bond orders between P and O atoms are from 0.46 to 0.75 e, between In and O atoms are from 0.29 to 0.35 e, and between Rb and O atoms are from 0.00 to 0.03 e in a unit cell of $RbInP_2O_7$ (pure covalence single bond order is generally 1.0 e). Accordingly, we can also say that the covalence strength is stronger for the P−O bond than the In−O bond, and ionic strength is stronger for the Rb−O bond than the In−O bond in $RbInP_2O_7$. The calculated bond orders and average atomic charges of $MInP_2O_7$ molecules within a unit cell are listed in Table 4. It is shown that the covalence strengths of the P−O bonds are stronger than those of the In−O bonds, and the M−O ionic interactions are the stronger in each ternary indium (III) pyrophosphate of $MInP_2O_7$ (M = Na, K, Rb, Cs).

3.3 Optical Properties. Figure 9a shows the absorption spectra of $MInP_2O_7$ (M = Na, K, Rb, Cs) determined from reflection measurements. From this figure we can see the strongest absorption peaks at about 180 nm (6.89 eV) and shoulder peaks at about 250 nm (4.96 eV) for $MInP_2O_7$ (M = Na, K, Rb, Cs). Wide transmission ranges from about 400 to 2000 nm for $MInP_2O_7$ are also found in this figure. As shown in Figure 9b, two broad emission spectra are obtained from 522 to 622 nm for $NaInP_2O_7$ and from 550 to 630 nm for $MInP_2O_7$ (M = Rb, Cs) when a light of wavelength 396 nm excites the pressed micro crystals. We also observe several weak emission peaks centered at about 688, 712, 766, and 824 nm for $MInP_2O_7$ (M = Na, Rb, and Cs).

Now, to evaluate and assign the observed spectra, we examine the linear optical response spectra of $MInP_2O_7$ crystals. The calculated imaginary $\epsilon_2(\omega)$ and the real $\epsilon_1(\omega)$ parts of the frequency-dependent dielectric functions are displayed in Figure 10. The part $\epsilon_2(\omega)$ can be used to describe the real transitions between occupied and unoccupied bands.

It is found from the dispersions of the calculated $\epsilon_2(\omega)$ spectra that there is a feature shoulder peak (first-

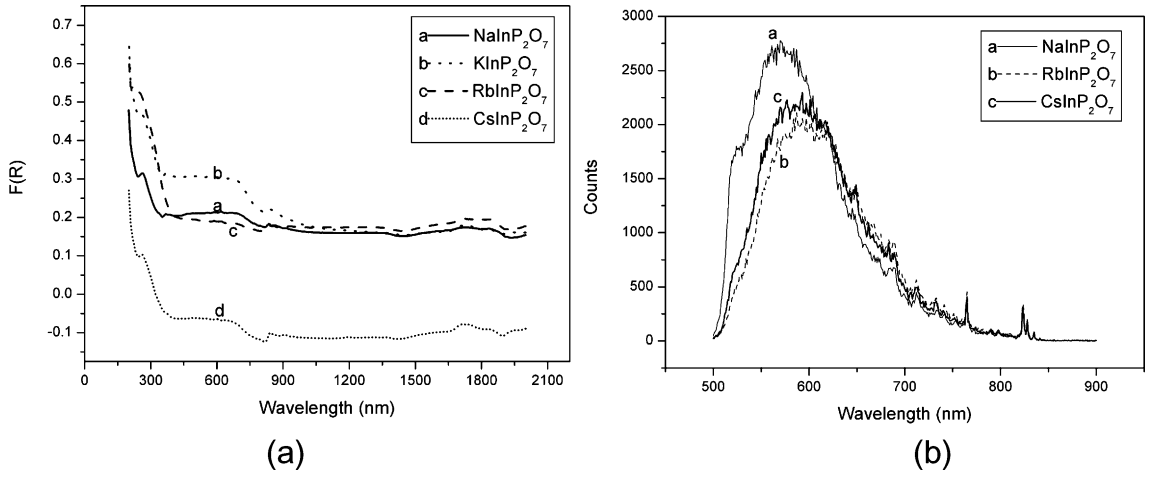

Figure 9. Observed (a) absorption and (b) emission spectra.

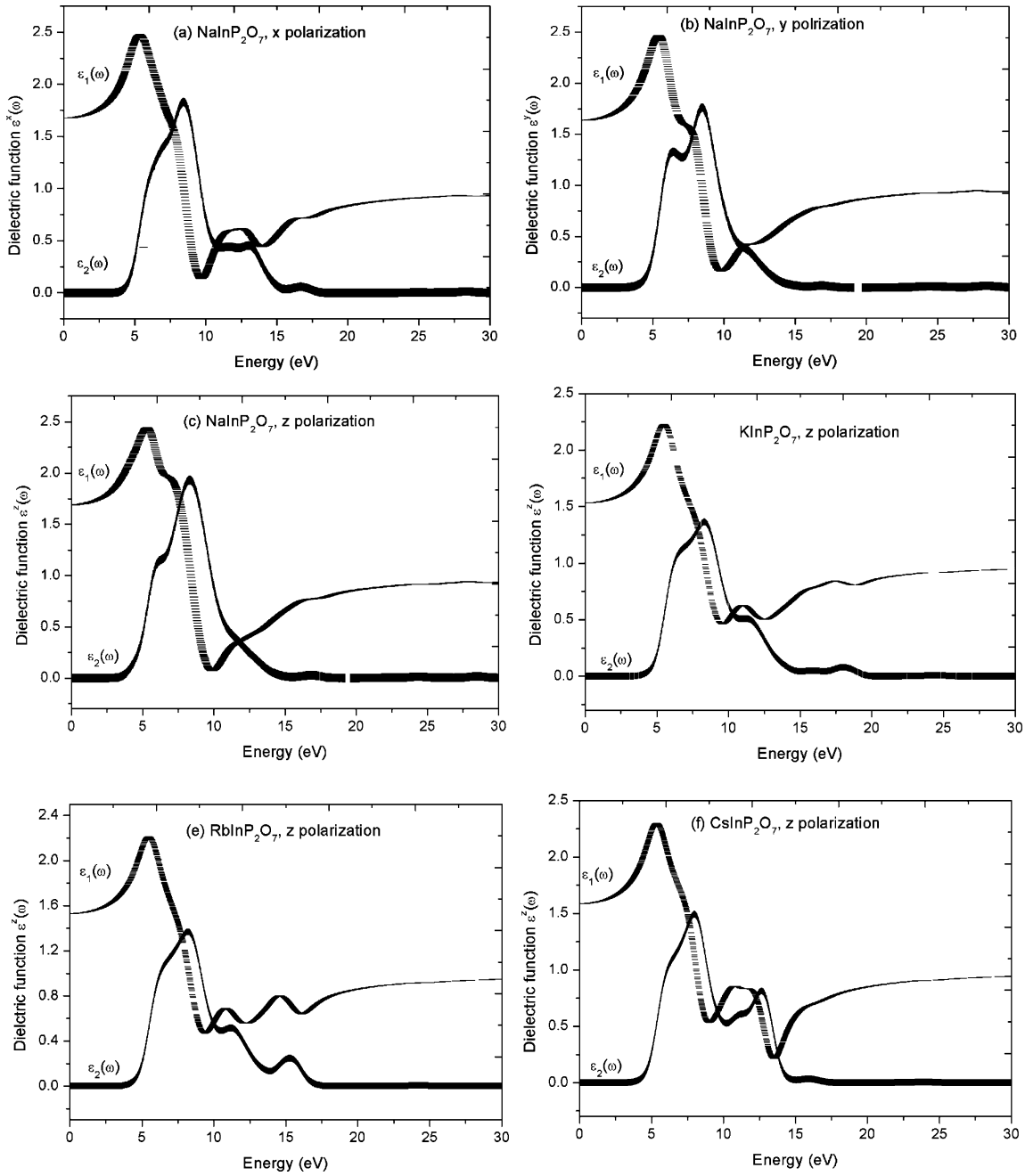

Figure 10. Calculated real and imaginary parts of dielectric functions.

absorption peak) at about 6.20 eV in each of the $MInP_2O_7$ (M = Na, K, Rb, Cs) crystals. These findings are similar to those of observed spectra localized at about 4.96 eV, as shown in Figure 9a. Accordingly, this shoulder peak (first absorption peak) is assigned as the charge transfers from O 2p π occupied states (near to Fermi energy) to In emptied states in terms of total and partial DOS analyses. The calculated strongest absorption peak (second-absorption peak) localized about 8.10 eV is compared with the observed one localized about 6.89 eV. The second-absorption peak is contribution from the charge transfers from hybridized states between the O 2p and P 3p states to In unoccupied states. Here we noted that the absorption peak positions localize at lower energy for the powders than the crystals and the UV transparent widths are smaller for the powders than the crystals. The calculated transparent cut-off edge is at about 350 nm shown in Figure 10 as compared with the observed one localized at about 400 nm (3.1 eV) shown in Figure 9a. It also assigns that the emission fluorescence of $MInP_2O_7$ originates from defects or excitons. This is due to the fact that the emitted energy of 2.4 eV (522 nm) is less than the optical absorption edge of about 3.1 eV, while we compare the absorption spectrum in Figure 9a with the emission spectrum in Figure 9b.

Dielectric constant is an important optical property. It is a measure of how fast light travels in a medium, and the lower the dielectric constant, the faster the speed of light. The calculated dielectric constants of static case, $\epsilon(0)$, i.e., $\epsilon_1(0)$, and the static first-order susceptibilities of different polarization directions are listed in Table 5for the $MInP_2O_7$ crystals. It is found that both the average dielectric constants of $\epsilon(0)$ and first-order susceptibilities increase in the order of $K^+ \approx Rb^+ < Cs^+$ for the $MInP_2O_7$ crystals (M = K, Rb, Cs).

Table 5. Calculated Dipole Electric Constants and First-Order Static Susceptibilities of $MInP_2O_7$

$MInP_2O_7$	$\epsilon_{xx}(0)$	$\epsilon_{yy}(0)$	$\epsilon_{zz}(0)$	$\chi^{(1)}_{xx}(0)$	$\chi^{(1)}_{yy}(0)$	$\chi^{(1)}_{zz}(0)$
M = Na	1.6738	1.6348	1.6906	0.05362	0.05052	0.05495
M = K	1.5509	1.5951	1.5325	0.04384	0.04735	0.04238
M = Rb	1.5570	1.5752	1.5301	0.04433	0.04578	0.04218
M = Cs	1.5785	1.5833	1.5856	0.04603	0.04642	0.04660

Table 6. Calculated Third-Order Static Susceptibilities of $MInP_2O_7$ Crystals (Unit: 10^{-14} esu)

$MInP_2O_7$	M = Na	M = K	M = Rb	M = Cs
$F_{cell}/10^{-9}$	2.5134	3.4834	3.8391	4.3416
$\chi^{(3)}_{xxxx}(0)$	6.2329	3.8602	4.4478	5.8470
$\chi^{(3)}_{yyyy}(0)$	4.9117	5.2530	5.0589	6.0477
$\chi^{(3)}_{zzzz}(0)$	6.8747	3.3711	3.6457	6.1421
$\chi^{(3)}_{xxyy}(0)$	1.8443	1.5010	1.5812	1.9822
$\chi^{(3)}_{xxzz}(0)$	2.1820	1.2024	1.3423	1.9976
$\chi^{(3)}_{yyzz}(0)$	1.9370	1.4027	1.4315	2.0316
$\langle\chi^{(3)}(0)\rangle^a$	5.9892	4.1393	4.3725	6.0119

[a] $\langle\chi^{(3)}(0)\rangle = 1/5[\chi^{(3)}_{xxxx}(0) + \chi^{(3)}_{yyyy}(0) + \chi^{(3)}_{zzzz}(0) + 2(\chi^{(3)}_{xxzz}(0) + \chi^{(3)}_{xxzz}(0) + \langle\chi^{(3)}(0)\rangle)]$.

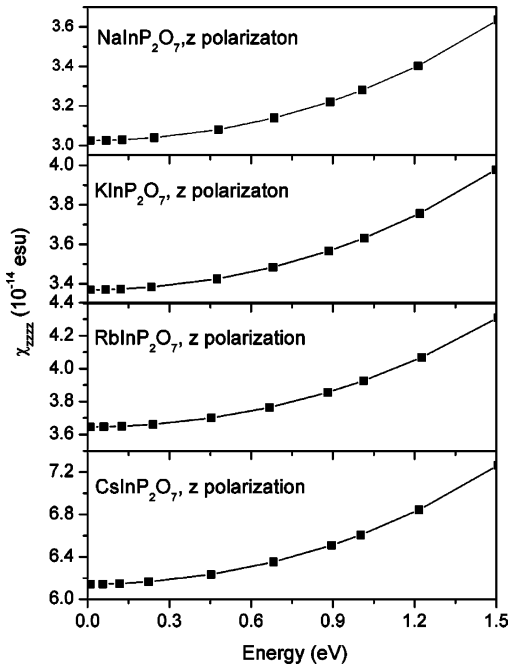

Figure 11. Calculated dynamic third-order optical susceptibilities of $MInP_2O_7$ by DFT-CAHO method.

The $NaInP_2O_7$ crystal is an exception in that the structure of $NaInP_2O_7$ with the eclipsed P_2O_7 groups and 6-sided tunnels is different from that of $MInP_2O_7$ (M = K, Rb, Cs) with the staggered P_2O_7 groups and 7-sided tunnels. As the dielectric constants of the $MInP_2O_7$ crystals have not been measured and reported, our calculated results listed in Table 4 only compare with the observed results of the other phosphate crystals. It is reported that the observed refractive index of phosphate is generally 1.40 ~1.60.[43] Our calculated refractive index of 1.27−1.30 derived from the dielectric constant is underestimated by about 12%.

Furthermore, we can calculate the third-order susceptibility from the first-order susceptibility by formula 2. CAHO provides a good description for those cases in which all of the optical frequencies are considerably smaller than the lowest electronic resonance frequency of the material system. This means that the optical transition energy is smaller than the band gap energy. The calculated susceptibility components at static case are listed in Table 6, and the dynamic susceptibilities of both polarization and foundation waves along with the z direction at low frequency are plotted in Figure 11 for the $MInP_2O_7$ crystals.

The F_{cell} in Table 5 is called the structural factor, and the $F_{cell} = (\omega_0^2/d^2 \cdot 1/n)m/(3N^3e^4)$ factors appear at formula 2 except $1/n$ in which n is the ion number within a unit cell. The factor n is introduced to give an average of oscillator ω_0 within a unit cell. It is expected that the average third-order susceptibilities of $MInP_2O_7$ crystals (M = K, Rb, Cs) increase as alkaline metal ionic radii increase except for the $NaInP_2O_7$ crystal, and the value of the $CsInP_2O_7$ crystal reaches about 6.0119×10^{-14} esu. As mentioned above, the exception of susceptibility of the $NaInP_2O_7$ crystal is due to the different arrangements of P_2O_7 groups in $NaInP_2O_7$ and $MInP_2O_7$ (M = K, Rb, Cs) crystals.

4. Conclusions

In this work, four pyrophosphates $MInP_2O_7$ (M = Na, K, Rb, Cs) have been synthesized by solid-state reaction and their structures have been determined by the single-crystal X-ray diffraction technique. These compounds crystallize in monoclinic system with space group $P2(1)/c$ and possess three-dimensional $(InP_2O_7)^-$ anionic frameworks with channels occupied by M^+ cations. The frameworks are built up from corner sharing of InO_6 octahedra and PO_4 tetrahedra. There are different arrangements of the tunnels between the $NaInP_2O_7$ and $MInP_2O_7$ (M = K, Rb, Cs). For the former, the tunnel running along [1 0 1] with 6-sided window is formed by the edges of two InO_6 octahedra and four PO_4 tetrahedra. For the latter, the tunnel running along [0 0 1] results from stacking of rings formed by the edges of three octahedra and four tetrahedra. The observed absorption and luminescence spectra of $MInP_2O_7$ (M = Na, K, Rb, Cs) microcrystals show the first absorption peak at about 260 nm for $MInP_2O_7$ (M = Na, K, Cs) and at 226 nm for $RbInP_2O_7$, and the broad emission spectra from 522 to 622 nm for $NaInP_2O_7$ and from 550 to 630 nm for $MInP_2O_7$ (M = Rb, Cs), respectively. The findings indicate that the emission fluorescence of $MInP_2O_7$ originates from defects or excitons. The calculated results of crystal band structures by the DFT method show that the solid compounds of $MInP_2O_7$ are insulators with direct band gaps of about 3.5 eV for $NaInP_2O_7$ and 3.7 eV for $MInP_2O_7$ (M = K, Rb, Cs) crystals. The calculated total and partial density of states indicate that the top valence bands are contributions from the mixings of O 2p and P 3p states and low conduction bands mostly originate from In^{3+} valence sates in the $MInP_2O_7$. The P−O bonds are substantial covalence features and In−O bonds are lesser ones, but the M−O bonds are almost ionic interactions. The observed first- and second-absorption peaks are assigned as the charge transfers from the O 2p π states and from the mixings between the O 2p and P 3p states to the In^{3+} valence states, respectively, for the $MInP_2O_7$. The calculated susceptibilities of the $MInP_2O_7$ crystal (M = Na, K, Rb,

(44) Dean, J. A., Ed. *Lange's Handbook of Chemistry*, 13th ed.; McGraw-Hill: New York, 1985.

Cs) increase as the alkaline metal element is from top to bottom in the periodic table with the exception of M = Na. The variation trends of energy gap and susceptibility of the $NaInP_2O_7$ is an exception among the $MInP_2O_7$ (M = Na, K, Rb, Cs) crystals. It is due to the different arrangements of the tunnels between the $NaInP_2O_7$ and $MInP_2O_7$ (M = K, Rb, Cs).

Acknowledgment. This investigation was based on work supported by the National Natural Science Foundation of China under projects 90201015 and 20373073, and the Science Foundation of the Fujian Province (E0210028 and 2002F010), and the Foundation of State Key Laboratory of Structural Chemistry (030060).

Supporting Information Available: Crystallographic data in CIF format for each of the four structures reported here. This material is available free of charge via the Internet at http://pubs.acs.org.

CM0491330